Research Article | Vol. 8, No. 2 | 1 Feb 2017 | BIOMEDICAL OPTICS EXPRESS 790

Biomedical Optics EXPRESS

Nanoparticle functionalised small-core suspended-core fibre – a novel platform for efficient sensing

BRENDA DOHERTY,[1,2,*] ANDREA CSÁKI,[1] MATTHIAS THIELE,[1] MATTHIAS ZEISBERGER,[1] ANKA SCHWUCHOW,[1] JENS KOBELKE,[1] WOLFGANG FRITZSCHE,[1] AND MARKUS A. SCHMIDT[1,2,3]

[1]*Leibniz Institute of Photonic Technology e.V., Albert-Einstein-Str. 9, 07745 Jena, Germany*
[2]*Abbe Center of Photonics, Friedrich-Schiller-University, Max-Wien-Platz, 1, 07743 Jena, Germany*
[3]*Otto Schott Institute of Material Research, Fraunhoferstr.6, Friedrich-Schiller-University, 07743 Jena, Germany*
[*]*brenda.doherty@leibniz-ipht.de*

Abstract: Detecting small quantities of specific target molecules is of major importance within bioanalytics for efficient disease diagnostics. One promising sensing approach relies on combining plasmonically-active waveguides with microfluidics yielding an easy-to-use sensing platform. Here we introduce suspended-core fibres containing immobilised plasmonic nanoparticles surrounding the guiding core as a concept for an entirely integrated optofluidic platform for efficient refractive index sensing. Due to the extremely small optical core and the large adjacent microfluidic channels, over two orders of magnitude of nanoparticle coverage densities have been accessed with millimetre-long sample lengths showing refractive index sensitivities of 170 nm/RIU for aqueous analytes where the fibre interior is functionalised by gold nanospheres. Our concept represents a fully integrated optofluidic sensing system demanding small sample volumes and allowing for real-time analyte monitoring, both of which are highly relevant within invasive bioanalytics, particularly within molecular disease diagnostics and environmental science.

OCIS codes: (060.2300) Fiber measurements; (060.2370) Fiber optics sensors; (060.4005) Microstructured fibers; (250.5403) Plasmonics; (280.4788) Optical sensing and sensors; (290.5850) Scattering, particles.

References and links

1. O. Lazcka, F. J. Del Campo, and F. X. Muñoz, "Pathogen detection: A perspective of traditional methods and biosensors," Biosens. Bioelectron. **22**(7), 1205–1217 (2007).
2. P. D'Orazio, "Biosensors in clinical chemistry - 2011 update," Clin. Chim. Acta **412**(19-20), 1749–1761 (2011).
3. S. M. Yoo and S. Y. Lee, "Optical Biosensors for the Detection of Pathogenic Microorganisms," Trends Biotechnol. **34**(1), 7–25 (2016).
4. A. G. Brolo, "Plasmonics for future biosensors," Nat. Photonics **6**(11), 709–713 (2012).
5. S. A. Maier and H. A. Atwater, "Plasmonics: Localization and guiding of electromagnetic energy in metal/dielectric structures," J. Appl. Phys. **98**(1), 011101 (2005).
6. J. Zhao, X. Zhang, C. R. Yonzon, A. J. Haes, and R. P. Van Duyne, "Localized surface plasmon resonance biosensors," Nanomedicine (Lond.) **1**(2), 219–228 (2006).
7. J. Cao, T. Sun, and K. T. V. Grattan, "Gold nanorod-based localized surface plasmon resonance biosensors: A review," Sens. Actuators B Chem. **195**, 332–351 (2014).
8. K. A. Willets and R. P. Van Duyne, "Localized surface plasmon resonance spectroscopy and sensing," Annu. Rev. Phys. Chem. **58**(1), 267–297 (2007).
9. M. Chamanzar, Z. Xia, S. Yegnanarayanan, and A. Adibi, "Hybrid integrated plasmonic-photonic waveguides for on-chip localized surface plasmon resonance (LSPR) sensing and spectroscopy," Opt. Express **21**(26), 32086–32098 (2013).
10. J. Homola, S. S. Yee, and G. Gauglitz, "Surface plasmon resonance sensors: review," Sens. Actuators B Chem. **54**(1-2), 3–15 (1999).
11. J. C. Yang, J. Ji, J. M. Hogle, and D. N. Larson, "Metallic nanohole arrays on fluoropolymer substrates as small label-free real-time bioprobes," Nano Lett. **8**(9), 2718–2724 (2008).
12. F. Eftekhari, C. Escobedo, J. Ferreira, X. Duan, E. M. Girotto, A. G. Brolo, R. Gordon, and D. Sinton, "Nanoholes As Nanochannels: Flow-through Plasmonic Sensing," Anal. Chem. **81**(11), 4308–4311 (2009).

#278810 http://dx.doi.org/10.1364/BOE.8.000790
Journal © 2017 Received 17 Oct 2016; revised 25 Dec 2016; accepted 27 Dec 2016; published 11 Jan 2017

Biomedical Optics EXPRESS

13. M. Barth, S. Schietinger, S. Fischer, J. Becker, N. Nüsse, T. Aichele, B. Löchel, C. Sönnichsen, and O. Benson, "Nanoassembled Plasmonic-Photonic Hybrid Cavity for Tailored Light-Matter Coupling," Nano Lett. **10**(3), 891–895 (2010).
14. A. Urrutia, J. Goicoechea, and F. J. Arregui, "Optical Fiber Sensors Based on Nanoparticle-Embedded Coatings," J. Sens. **2015**, 1–18 (2015).
15. J. Luo, J. Yao, Y. Lu, W. Ma, and X. Zhuang, "A Silver Nanoparticle-Modified Evanescent Field Optical Fiber Sensor for Methylene Blue Detection," Sensors (Basel) **13**(3), 3986–3997 (2013).
16. A. M. Aravanis, L. P. Wang, F. Zhang, L. A. Meltzer, M. Z. Mogri, M. B. Schneider, and K. Deisseroth, "An optical neural interface: in vivo control of rodent motor cortex with integrated fiberoptic and optogenetic technology," J. Neural Eng. **4**(3), S143–S156 (2007).
17. S. Faez, Y. Lahini, S. Weidlich, R. F. Garmann, K. Wondraczek, M. Zeisberger, M. A. Schmidt, M. Orrit, and V. N. Manoharan, "Fast, label-free tracking of single viruses and weakly scattering nanoparticles in a nano-fluidic optical fiber," ACS Nano **9**(12), 12349–12357 (2015).
18. M. A. Schmidt, A. Argyros, and F. Sorin, "Hybrid Optical Fibers – an innovative platform for in-fiber photonic devices," Adv. Opt. Mater. **4**(1), 13–36 (2016).
19. T. Wieduwilt, A. Tuniz, S. Linzen, S. Goerke, J. Dellith, U. Hubner, and M. A. Schmidt, "Ultrathin niobium nanofilms on fiber optical tapers - a new route towards low-loss hybrid plasmonic modes," Sci. Rep. **5**, 17060 (2015).
20. T. Wieduwilt, K. Kirsch, J. Dellith, R. Willsch, and H. Bartelt, "Optical Fiber Micro-Taper with Circular Symmetric Gold Coating for Sensor Applications Based on Surface Plasmon Resonance," Plasmonics **8**(2), 545–554 (2013).
21. T. Wieduwilt, M. Zeisberger, M. Thiele, B. Doherty, M. Chemnitz, A. Csaki, W. Fritzsche, and M. A. Schmidt, "Gold-reinforced silver nanoprisms on optical fiber tapers—A new base for high precision sensing," APL Photonics **1**(6), 066102 (2016).
22. J. Cao, E. K. Galbraith, T. Sun, and K. T. V. Grattan, "Cross-Comparison of Surface Plasmon Resonance-Based Optical Fiber Sensors With Different Coating Structures," IEEE Sens. J. **12**(7), 2355–2361 (2012).
23. H. Y. Lin, C. H. Huang, G. L. Cheng, N. K. Chen, and H. C. Chui, "Tapered optical fiber sensor based on localized surface plasmon resonance," Opt. Express **20**(19), 21693–21701 (2012).
24. T. G. Euser, J. S. Y. Chen, M. Scharrer, P. S. J. Russell, N. J. Farrer, and P. J. Sadler, "Quantitative broadband chemical sensing in air-suspended solid-core fibers," J. Appl. Phys. **103**(10), 103108 (2008).
25. S. C. Warren-Smith, J. Wie, M. Chemnitz, R. Kostecki, H. Ebendorff-Heidepriem, T. M. Monro, and M. A. Schmidt, "Third harmonic generation in exposed-core microstructured optical fibers," Opt. Express **24**(16), 17860–17867 (2016).
26. A. M. Cubillas, S. Unterkofler, T. G. Euser, B. J. M. Etzold, A. C. Jones, P. J. Sadler, P. Wasserscheid, and P. S. Russell, "Photonic crystal fibres for chemical sensing and photochemistry," Chem. Soc. Rev. **42**(22), 8629–8648 (2013).
27. G. O. S. Williams, J. S. Y. Chen, T. G. Euser, P. S. Russell, and A. C. Jones, "Photonic crystal fibre as an optofluidic reactor for the measurement of photochemical kinetics with sub-picomole sensitivity," Lab Chip **12**(18), 3356–3361 (2012).
28. A. Csáki, F. Jahn, I. Latka, T. Henkel, D. Malsch, T. Schneider, K. Schröder, K. Schuster, A. Schwuchow, R. Spittel, D. Zopf, and W. Fritzsche, "Nanoparticle Layer Deposition for Plasmonic Tuning of Microstructured Optical Fibers," Small **6**(22), 2584–2589 (2010).
29. K. Schroder, A. Csaki, A. Schwuchow, F. Jahn, K. Strelau, I. Latka, T. Henkel, D. Malsch, K. Schuster, K. Weber, T. Schneider, R. Moller, and W. Fritzsche, "Functionalization of Microstructured Optical Fibers by Internal Nanoparticle Mono-Layers for Plasmonic Biosensor Applications," IEEE Sens. J. **12**(1), 218–224 (2012).
30. A. Schwuchow, M. Zobel, A. Csáki, K. Schröder, J. Kobelke, W. Fritzsche, and K. Schuster, "Monolayers of different metal nanoparticles in microstructured optical fibers with multiplex plasmonic properties," Opt. Mater. Express **2**(8), 1050–1055 (2012).
31. K. M. Mayer and J. H. Hafner, "Localized Surface Plasmon Resonance Sensors," Chem. Rev. **111**(6), 3828–3857 (2011).
32. F. Warken, E. Vetsch, D. Meschede, M. Sokolowski, and A. Rauschenbeutel, "Ultra-sensitive surface absorption spectroscopy using sub-wavelength diameter optical fibers," Opt. Express **15**(19), 11952–11958 (2007).
33. H. Ebendorff-Heidepriem, S. C. Warren-Smith, and T. M. Monro, "Suspended nanowires: Fabrication, design and characterization of fibers with nanoscale cores," Opt. Express **17**(4), 2646–2657 (2009).
34. X. C. Yu, B. B. Li, P. Wang, L. Tong, X. F. Jiang, Y. Li, Q. Gong, and Y. F. Xiao, "Single Nanoparticle Detection and Sizing Using a Nanofiber Pair in an Aqueous Environment," Adv. Mater. **26**(44), 7462–7467 (2014).
35. G. M. Whitesides, "The origins and the future of microfluidics," Nature **442**(7101), 368–373 (2006).
36. J. Turkevich, P. C. Stevenson, and J. Hillier, "A Study of the Nucleation and Growth Processes in the Synthesis of Colloidal Gold," Discuss Faraday Soc, 55 (1951).
37. G. Frens, "Controlled Nucleation for Regulation of Particle-Size in Monodisperse Gold Suspensions," Nature-Phys Sci **241**(105), 20–22 (1973).

Biomedical Optics EXPRESS

38. A. M. Cubillas, M. Schmidt, T. G. Euser, N. Taccardi, S. Unterkofler, P. St. J. Russell, P. Wasserscheid, and B. J. M. Etzold, "In Situ Heterogeneous Catalysis Monitoring in a Hollow-Core Photonic Crystal Fiber Microflow Reactor," Adv. Mater. Interfaces **1**(5), 1300093 (2014).
39. S. A. Maier, M. L. Brongersma, P. G. Kik, and H. A. Atwater, "Observation of near-field coupling in metal nanoparticle chains using far-field polarization spectroscopy," Phys. Rev. B **65**(19), 193408 (2002).
40. A. Csáki, M. Thiele, J. Jatschka, A. Dathe, D. Zopf, O. Stranik, and W. Fritzsche, "Plasmonic nanoparticle synthesis and bioconjugation for bioanalytical sensing," Eng. Life Sci. **15**(3), 266–275 (2015).
41. Alexandre Dmitriev, ed., *Nanoplasmonic Sensors* (Springer, 2012).
42. A. Hassani, B. Gauvreau, M. F. Fehri, A. Kabashin, and M. Skorobogatiy, "Photonic crystal fiber and waveguide-based surface plasmon resonance sensors for application in the visible and near-IR," Electromagnetics **28**(3), 198–213 (2008).
43. A. Hassani and M. Skorobogatiy, "Design criteria for microstructured-optical-fiber-based surface plasmon-resonance sensors," J. Opt. Soc. Am. B **24**(6), 1423–1429 (2007).
44. N. J. Florous, K. Saitoh, and M. Koshiba, "Numerical modeling of cryogenic temperature sensors based on plasmonic oscillations in metallic nanoparticles embedded into photonic crystal fibers," IEEE Photonics Technol. Lett. **19**(5), 324–326 (2007).
45. M. Hautakorpi, M. Mattinen, and H. Ludvigsen, "Surface-plasmon-resonance sensor based on three-hole microstructured optical fiber," Opt. Express **16**(12), 8427–8432 (2008).
46. A. Steinbrück, A. Csaki, and W. Fritzsche, "Metal Nanoparticles for Molecular Plasmonics," Reviews in Plasmonics **2010**, 1–37 (2010).

1. Introduction

The non-invasive detection of life-threatening disease is a major challenge in biomedicine, since it requires identifying pathogens of extremely low concentration or even on the single molecular level [1–3]. One promising detection strategy providing such sensitivity and selectivity, without the necessity of molecular labelling, relies on attaching molecular probes to metallic nanoparticles (NPs) [4]. The electron ensemble of such NPs is collectively excited by an external electromagnetic wave at a characteristic wavelength, creating localised surface plasmon resonances (LSPRs) [5]. Functionalising NPs with specific molecular probes then allows detection of molecular binding events via a macroscopic change of the plasmonic resonance [6–9]. Many of the currently used plasmonic devices rely on planar fabrication technology, i.e. planar integrated photonic structures, examples of which include nanohole arrays, nanochannel flow-through sensing, and hybrid optical cavities [10–13]. Despite their success, these devices can show limited device performance due to short light-matter interaction lengths, complex and inefficient launching schemes, and intrinsically high optical loss.

An alternative approach places plasmonic NPs into the evanescent fields of the modes of optical fibres [14,15]. Fibre platforms in general offer profound advantages particularly with respect to bioanalytical application such as: spectral and spatial multiplexing, flexible handling, precise control of modal properties, and the potential for in-vivo applications [16–18]. So far almost all fibre-integrated plasmonic sensors involve multi- or single-mode optical tapers which have been coated either with continuous metallic nanofilms [19,20] or plasmonic NPs [21–23]. Although these systems have displayed refractive index (RI) sensing capabilities, the NPs are located on the outer surface of the taper, yielding non-integrated and delicate-to-handle devices with further disadvantages including the requirement for large analyte volumes with only a fraction used for the actual sensing.

An important class of novel optical fibres, possessing great potential within the field of bioanalytics, are suspended-core fibres (SCFs) (Fig. 1) [24,25]. These microstructured fibres contain axial air channels which extend along the entire fibre length and have diameters of several tens of micrometres. Typically three or four of these channels are arranged such to form a central micrometre-size glass core resembling the geometry of a step index fibre, with the propagating mode deeply penetrating into the channel via its evanescent field. These fibres are particularly attractive from the bioanalytical perspective, as they allow real-time probing of liquid analytes flowing through the channel regions by using the light propagating inside the fibre core. Promising experiments indicate successful application of analytics in SCFs, examples of which include sensing of ionic liquid [24,26] and dynamic detection of

Biomedical Optics EXPRESS

trans/cis isomerisation processes [27]. First attempts to integrate small metallic NPs into SCFs have been recently conducted [28–30], wherein the LSPRs were probed perpendicular to the fibre axis, which does not exploit the advantage of the fibre geometry.

Here we show that a nanoparticle-functionalised suspended core fibre can act as a highly integrated optofluidic platform for efficient RI sensing. Due to the small core diameter, we obtain strong interaction of plasmon and guided mode, allowing us to access two orders of magnitude of nanoparticle densities at moderate sample lengths. The measured sensitivity is of the same order compared to particles in solution, making this monolithic system highly attractive for applications within bioanalytics [31].

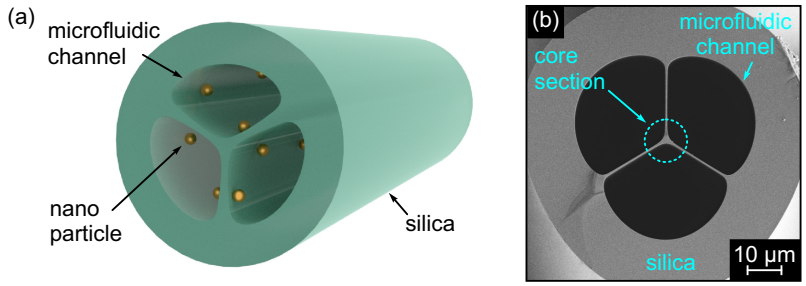

Fig. 1. (a) Schematic of the plasmonic nanoparticle-functionalised suspended-core fibre. (b) Scanning-electron micrograph (SEM) of the microstructured section of the investigated fibre. Grey areas correspond to silica glass, the black regions to air. The dashed cyan circle highlights the core section relevant for the interaction between light and localised surface plasmons.

2. Working principle

The fundamental working principle of NP-enhanced SCFs relies on the interaction of the propagating guided mode with the LSPR of the NPs, whereby the characteristics of the plasmonic resonance are impressed on the spectral distribution of the transmitted light. Therefore a spectral shift of the LSPR imposed by, for instance, a change of the nanoscale RI environment of the NP, will be visible in the modal attenuation spectrum.

The modal attenuation can be calculated by a line integration of the area of the mode along the surface of the SCF core, taking into account the extinction cross section and the density of the NPs [21,32], leading to

$$\gamma = N\sigma\oint A_{eff}^{-1}dl \tag{1}$$

with the number density of the NPs and the extinction cross section, N and σ, respectively, and the effective modal scattering area on the surface A_{eff}. The latter quantity is defined by

$$A_{eff}(\vec{r}_0) = \frac{\int_{A_\infty} S_z(\vec{r})dA}{S_z(\vec{r}_0)} \tag{2}$$

with the axial Poynting vector of the guided mode $S_z(\vec{r})$ and the position of the NP on the surface of the core $(\vec{r}_0)$. This parameter is essential for analysing NP scattering on waveguide systems, with the ratio $f = \sigma/A_{eff}$ referring to the fraction of power removed from the propagating mode by one single NP scattering event. Consequently, detecting objects with small extinction cross sections or investigating systems with low NP densities generally requires small core sizes to obtain sufficiently low values of A_{eff}.

Using finite element simulation we calculated the spectral distribution of A_{eff} for the SCF fibre geometry investigated here (Fig. 1b) and compared it to a cylindrical silica taper in water with a diameter based on the definition given in Ref [24,33]. It is assumed that the NP is located 1 nm above the glass surface in one hole of the SCF (Fig. 2). Smaller values of A_{eff} are

Biomedical Optics EXPRESS

achieved at longer wavelength due to the larger field modal penetration into the analyte (Fig. 2), suggesting that the optimal operating regime of such kind of sensor device is at longer wavelengths.

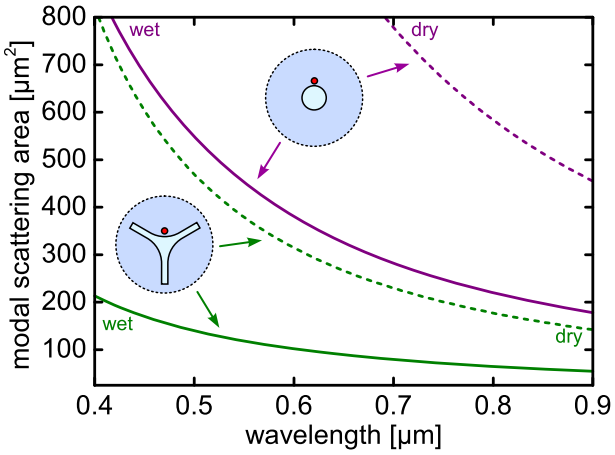

Fig. 2. Comparison of the spectral distributions of the effective modal scattering areas for the 2.8 µm diameter suspended-core fibre investigated here (green curve) and a circular silica taper embedded in water with a diameter of 3.62 µm (purple curve). The dashed and solid lines refer to air or water as analyte medium, respectively. It is assumed that the particle is located 1 nm above the glass surface as indicated by the red dots in the sketches.

Theoretically, a single spherical gold NP of diameter 34 nm at resonance in water (550 nm, $\sigma = 2 \cdot 10^{-3}$ µm^2) would impose a comparably small reduction of guided power of $f = 1.62 \cdot 10^{-5}$ ($A_{eff} = 120$ µm^2), whereas for instance a 1µm-diameter polymer bead ($\sigma = 1.5$ µm^2) reduces the guided power by as much as 1.2%. The latter shows that such small core systems provide a sufficient platform to detect single microparticles [34]. It is interesting to note that the effective modal scattering area of the SCF is almost a factor of three smaller than that of a corresponding taper when using the core diameter definition of Ref [33], emphasising the excellent performance of the SCF platform with regard to sensing.

Equation (1) allows the estimation of the relative change of modal attenuation when exchanging the analyte medium. Simulations of extinction cross section (using the NPs considered here) and modal scattering area reveal an increase of σ upon changing the analyte from air to water, whereas a higher analyte RI imposes a decrease in A_{eff} which is more pronounced at shorter wavelengths (Fig. 2). To obtain a rough estimate of the change of the attenuation, we chose here $\lambda = 700$ nm, which is sufficiently distant from the plasmon resonance. Using the parameters at that wavelength ($\sigma_{air} = 0.012$ NPs/µm^2, $\sigma_{water} = 0.038$ NPs/µm^2, $A_{eff}^{water} = 80$ µm^2, $A_{eff}^{air} = 230$ µm^2), a change of modal attenuation of $\Delta\gamma = \gamma_{air} / \gamma_{water} \approx 0.11$ is calculated, implying that the modal attenuation is about a factor 9 higher in case of an aqueous analyte compared to the situation where the cladding medium is air ($\gamma_{water} > \gamma_{air}$).

3. Fibre geometry

The suspended fibre geometry used here consists of three air channels with diameters of several tens of micrometres surrounding a triangular silica core (Figs. 1(a) and 1(b)). The fabrication of this type of fibre relies on stacking three capillaries into a silica jacketing tube and drawing this arrangement into fibre. The diameter of the core section is approximately 2.8 µm (based on the definition given in Ref [24,33].), which is a small value compared to typically used NP functionalised fibre systems (e.g., tapers) [7,23]. The core section is suspended by three struts of approximate thickness 500 nm. The holes adjacent to the core

Biomedical Optics EXPRESS

have shapes close to that of 120° circular section with an area of approximately 1,500 μm^2, which is of the same area as the channels in typical microfluidic devices [35].

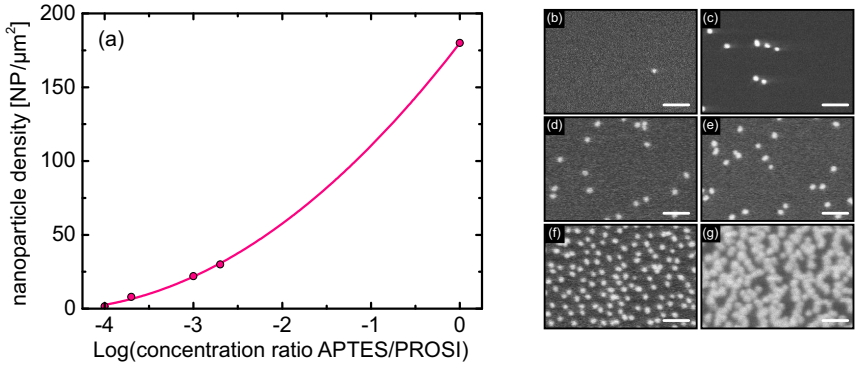

Fig. 3. (a) Density of the nanospheres inside the suspended-core fibre as a function of the concentration ratio of APTES and PROSI (pink points) used. The solid line is a parabolic fitting curve (parameters given in the text). The right-handed images ((b)-(g)) are SEM images of the various achieved densities inside one hole of the respective suspended-core fibre (b: 2 NPs/μm^2; c: 8 NPs/μm^2; d: 22 NPs/μm^2; e: 30 NPs/μm^2; f: 180 NPs/μm^2; g: 500 NPs/μm^2. The scale bars in (b) to (f) correspond to 200 nm and in (g) to 100 nm.

4. Fabrication – NP deposition

The various NP densities (Figs. 3(b)-3(g)) were realised using a nanoparticle layer deposition (NLD) technique as implemented in Refs [28,29]. This is a dynamic low-pressure chemical deposition based on self-assembled monolayers, using amino modification of the interior channel surfaces as adhesive layers for the NPs.

The empty SCF is connected to a peristaltic pump with PVC tubes and microfluidic adaptors for the delivery and exchange of liquids. Following the cleaning and activation of the interior silica surface, the subsequent silane modification involves the perfusion of a ratio of bonding and nonbonding silane volumes, namely (3-Aminopropyl)triethoxysilane (APTES, containing amino group) and n-propyltriethoxysilane (PROSI) respectively (Sigma-Aldrich), whereby the actual volume ratio of APTES and PROSI, Δc, allows control of the NP density inside the channels. The NP solution (Au Nanospheres 34 nm, fabricated by Turkevich-Frens Method [36,37]) is then introduced into the functionalised channels with a low flow rate, allowing the immobilisation of NPs along the entire SCF length.

Up to 6 m coverages of NPs inside the SCF, with homogeneous nanoparticle density (confirmed by taking short sample sections from along the length of the deposited fibre and SEM imaging the pieces' interiors at their end faces), have been achieved independent of the curvature of the channels. The obtained homogeneity compares well with a recently presented deposition approach, over 50cm, relying on directly synthesizing Rh-NPs at the inner walls of a hollow-core optical fibre through reduction of metallic precursor in a gaseous atmosphere [38]. The resulting dependence of NP density on APTES/PROSI ratio yields a curve fit, $N = A + B\log_{10}\Delta c + C(\log_{10}\Delta c)^2$ with the constants A = 179.95 NPs/μm^2, B = 78.00 NPs/μm^2 and C = 8.41 NPs/μm^2, allowing a guideline for tailored density depositions.

Biomedical Optics EXPRESS

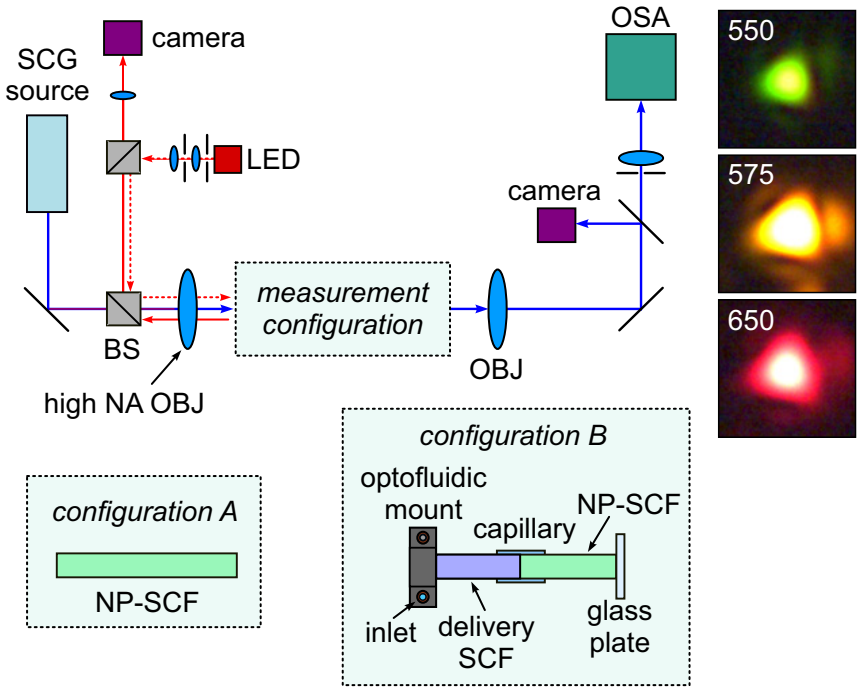

Fig. 4. Schematic of the optofluidic setup used to measure the transmission through the nanoparticle-functionalised suspended-core fibre (SCG: supercontinuum generation; BS: beam splitter; OBJ: objective; OSA: optical spectrum analyzer). The blue arrows refer to the probe light used to determine the transmission characteristics. The red arrows correspond to the light used for imaging the spot of the beam on the input facet of the sample (dashed red lines: illumination light, solid red lines: reflected light). The lower two sketches show the two different measurement configurations used for the quantification of the modal attenuation (configuration A) and for the determination of the refractive index sensitivity (configuration B). The right-handed images show the output mode at selected wavelength for a sample with N = 22 NP/μm^2 (top: 550 nm, middle: 575 nm, bottom: 650 nm) in the case of microchannels filled with air.

5. Experimental

The experimental setup used herein consists of a broadband transmission setup, including an optofluidic sample holder for the simultaneous excitation of the core mode and analyte exchange within the microstructured channels (Fig. 4).

The broadband light (450 nm to 2.4 μm) emitted from a supercontinuum source (SuperK COMPACT, NKT Photonics) passes a beam splitter and the front window of the optofluidic mount and is launched into the fibre core with a high-NA objective (Nikon TU Plan Fluor, 100x objective, NA 0.9). The output mode is either coupled into an optical spectrum analyzer (OSA) or imaged onto a combination of a camera and a narrow bandpass filter to select the wavelength to be imaged. To ensure optimal launching conditions, the spot of the input beam on the fibre front facet is imaged onto a camera using various lenses and a Köhler illumination. This setup ensures excitation of a clean fundamental mode in the SCF for all relevant wavelengths (modal images at selected wavelengths are shown on the right-handed side of Fig. 4).

The modal attenuation has been determined by applying the cutback technique on each of the NP-functionalised fibre samples when the channels are filled with air. Using the aforementioned setup without the optofluidic mount (Fig. 4, configuration A), the fibre end-facet was repeatedly cleaved and the corresponding spectra recorded (typically 4-5 measurements). Due to the high scattering induced by the NPs and the limited dynamic range of the OSA, cutback measurements were performed on short sample lengths, typically starting

Biomedical Optics EXPRESS

at 1 cm and ending 2 mm. Fibre samples with lower densities allowed longer working lengths (up to 9 cm) however the greater plasmonic effect was observed for higher densities.

To determine the RI sensitivity of the deposited SCFs, a sample with a NP density of 22 NPs/μm^2 was chosen, which represents a compromise between strong plasmon/waveguide mode interaction (i.e., short samples) and an reasonable sample length of about 1-2 cm. Using the abovementioned setup (Fig. 4, configuration B) the SCF was flushed with different RI oils (Oil series AAA, Cargille Laboratories) using a pressurised syringe pump. To avoid difficulties (i.e, sample breakage) involved during mounting and flushing a sample of such short length, an uncoated delivery SCF was butt-coupled to the NP-functionalised sample, with the joining point sealed within a 140 μm capillary while optimising the output mode and transmission. The empty SCF end was then fixed within the input optofluidic mount, ensuring stable and reproducible launching conditions with no significant increase of the overall modal attenuation. The individual RI oil was pumped through the fluidic holder and fibre system until all air bubbles (detectable on camera) were eliminated. A coverslip at the output end of the NP-fibre ensured a flat transmission face, which is essential for efficiently coupling the light into the OSA. Between each spectral series, the system was rinsed (pump and suction) repeatedly with ethanol and air bubbles induced, in order to eliminate remnants of the previous analyte.

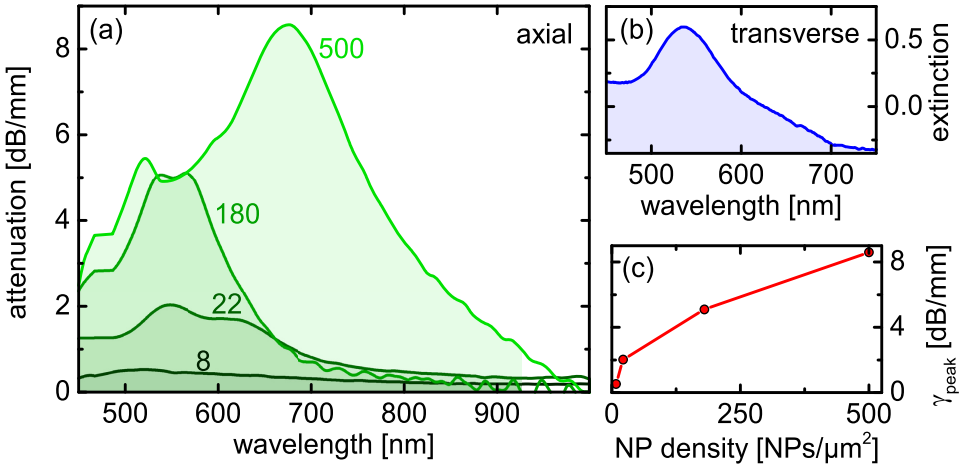

Fig. 5. (a) Measured spectral distribution of the attenuation of the fundamental core mode in the nanoparticle-functionalised suspended-core fibre (microchannels filled with air). The various curves correspond to different nanoparticle densities (most dark green: 8 NPs/μm^2; dark green: 22 NPs/μm^2; green: 180 NPs/μm^2; light green: 500 NPs/μm^2). (b) Extinction spectrum of the used nanoparticle ensemble in the case where the nanoparticles are probed transverse to the fibre axis in water (bulk measurement, N = 180 NPs/μm^2). (c) Modal attenuation at the most prominent attenuation peak of the individual attenuation curve in (a) as function of nanoparticle density.

6. Result

The spectral distribution of the modal attenuation of the NP-functionalised SCF shows a strong increase in the spectral vicinity of the bulk LSPR (Figs. 5(a) and 5(b)). As suggested by Eq. (1) an increasing NP density leads to increasing modal attenuation (Fig. 5(c)), whereas due to the small core diameter both extremely small NP densities (2 NPs/μm^2) as well as very high coverages of up to 500 NPs/μm^2 can be accessed with our device. Particularly for the two highest coverage densities the average inter-particle edge-to-edge distance (gap size) g is of the order of several tens of nanometres only (180 NPs/μm^2 – g = 40 nm, 500 NPs/μm^2 – g = 10 nm, Figs. 3(f) and 3(g)) which allows the LSPRs of neighbouring NPs to interact, overall imposing that the linear dependency between density and attenuation defined in Eq. (1) does not hold (Fig. 5(c)). The samples with the two highest densities show pronounced double peak

Biomedical Optics EXPRESS

features, which presumably arise from both the interaction of neighbouring particles (i.e., plasmonic hybridization) and the polarisation dependence of the scattering process, since the dominant electric field component of the guided mode is different at the various NP locations along the core surface. As shown in [39] the coupling of adjacent particles causes a red shift for in-plane electric fields and a blue shift for out-of-plane fields with closer NPs imposing a stronger shift as confirmed in the experiment presented here.

The RI sensitivity measurements, which have been conducted by pumping various RI oils (series AAA, Cargille Laboratories) into the microchannels of the SCF, show an increase of the wavelength of the transmission dip for higher analyte indices (Fig. 6), which is a result of the shift of the LSPR of the NPs towards longer wavelength (inset of Fig. 6, details of the sensing experiments can be found in the Experimental section (Sec. 5)). Linear fitting of the data points yields a RI sensitivity of 167 nm/RIU, which is within the typically range of sensitivity values of spherical plasmonic NPs [40] and is about 1.5 times higher than the corresponding value when the LSPR are probed transverse to the fibre axis (inset of Fig. 6).

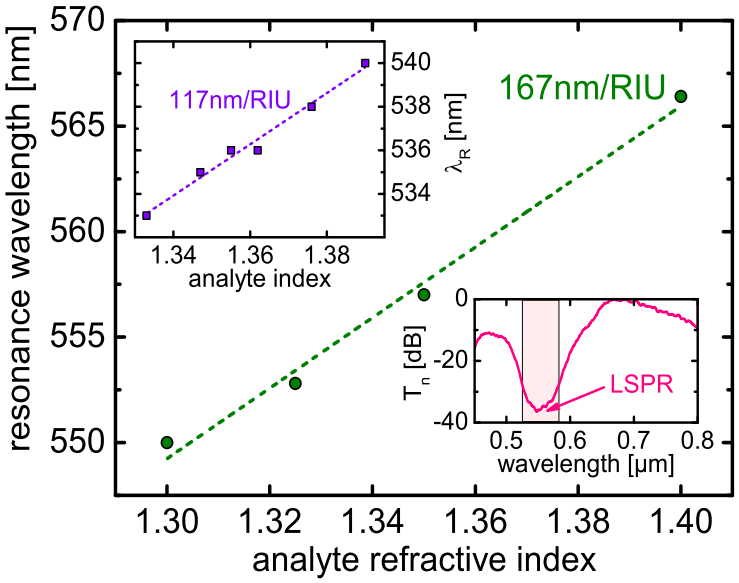

Fig. 6. Measured shift of the resonance wavelength as function of analyte refractive index for a fibre sample with a density of 22 NPs/μm^2 and a length of 4 mm, yielding a sensitivity of 167 nm/RIU. The upper left-hand inset (purple) shows the corresponding plot of nanospheres in aqueous solution when the incident light is perpendicular to the fibre axis (transverse measurement configuration), giving rise to a sensitivity of 117nm/RIU. The lower right-hand inset (pink) shows an example transmission spectrum in the case of a water analyte (normalised to the highest transmission value, light red area indicates the region of the LSPR). Note that this curve includes the spectral characteristics of the various components of the measurement setup (e.g., light source).

7. Conclusion

The specific detection of target species is of major importance within bioanalytics, in particular from the perspective of disease diagnostics. One promising method is to sense molecular binding events via the shift of plasmonic resonances of metallic nanoparticles, which strongly respond to changes in the nanoscale refractive index environment. Ideally this approach combines a monolithic microfluidic platform with an optical waveguide [41–45], where the nanoparticles should be located as close as possible to the guiding core.

Here we introduce the concept of suspended-core fibres with immobilised nanoparticles as an integrated optofluidic platform for efficient refractive index sensing over two orders of magnitude of nanoparticle density. Due to the small guiding core and the microfluidic

Biomedical Optics EXPRESS

channels being in direct contact with that core over a distance of several centimetres, intense interaction of localised plasmons and propagating mode is observed, allowing us to investigate sparse particle ensembles as well as ensembles with extremely high densities. Furthermore, the direct immobilisation of nanoparticles allows for a reusable sensing system.

The core, which to our knowledge has the smallest diameter being used for NPs immobilisation so far, is fully encapsulated inside the fibre and supported by radial strands, leading to superior handling properties compared to freely-suspended waveguide systems such as tapers. The refractive index sensitivity of our sensor when functionalised with gold nanospheres of average diameter 34 nm was measured as 170 nm/RIU for an aqueous analyte, that being 1.5 times higher compared to measurements taken perpendicular to the fibre axis (transverse configuration, upper left-hand inset in Fig. 6) and to sensitivity values of similar NPs dispersed in water [46].

Due to the small core sizes and the integrated arrangement of optical core and microfluidic channels our fibre represents a fully integrated optofluidic sensing system requiring only small sample volumes and allowing for real-time monitoring of the analyte. Therefore we anticipate application of our concept within the area of non-invasive bioanalytics, particular within molecular disease diagnostics and environmental science.

Funding

The authors gratefully acknowledge financial support from the DFG (SCHM2655/3-1) and the Thuringian State (projects 2015FGI0011, 2015-0021) partly supported by the European Social Funds (ESF).